

# UCLA

## UCLA Previously Published Works

### Title

Inhibiting amyloid  $\beta$ -protein assembly: Size-activity relationships among grape seed-derived polyphenols

### Permalink

<https://escholarship.org/uc/item/84c655x1>

### Journal

Journal of Neurochemistry, 135(2)

### ISSN

0022-3042

### Authors

Hayden, EY  
Yamin, G  
Beroukhim, S  
et al.

### Publication Date

2015-10-01

### DOI

10.1111/jnc.13270

Peer reviewed

ORIGINAL  
ARTICLEInhibiting amyloid  $\beta$ -protein assembly:  
Size–activity relationships among grape  
seed-derived polyphenols

Eric Y. Hayden,<sup>\*,1</sup> Ghiam Yamin,<sup>\*,†,1,2</sup> Shiela Beroukhim,<sup>\*</sup> Benson Chen,<sup>\*</sup> Mikhail Kibalchenko,<sup>\*</sup> Lin Jiang,<sup>\*</sup> Lap Ho,<sup>‡</sup> Jun Wang,<sup>‡,§,¶</sup> Giulio M. Pasinetti,<sup>‡,§,¶</sup> and David B. Teplow<sup>\*,\*\*\*</sup>

<sup>\*</sup>Department of Neurology, David Geffen School of Medicine, University of California, Los Angeles, California, USA

<sup>†</sup>Medical Scientist Training Program, Neuroscience Interdepartmental Ph.D. Program, University of California, Los Angeles, California, USA

<sup>‡</sup>Departments of Psychiatry and Neuroscience, Icahn School of Medicine at Mount Sinai, One Gustave L. Levy Place, New York, New York, USA

<sup>§</sup>Department of Neurology, Icahn School of Medicine at Mount Sinai, One Gustave L. Levy Place, New York, New York, USA

<sup>¶</sup>Geriatric Research, Education and Clinical Center (GRECC), James J. Peters Veterans Affairs Medical Center, 130 West Kingsbridge Road, Bronx, New York, USA

<sup>\*\*\*</sup>Molecular Biology Institute (MBI), and Brain Research Institute (BRI), David Geffen School of Medicine, University of California, Los Angeles, California, USA

**Abstract**

Epidemiological evidence that red wine consumption negatively correlates with risk of Alzheimer's disease has led to experimental studies demonstrating that grape seed extracts inhibit the aggregation and oligomerization of A $\beta$  *in vitro* and ameliorate neuropathology and behavioral deficits in a mouse model of Alzheimer's disease. The active agent in the extracts is a mixed population of polyphenolic compounds. To evaluate the relative potency of each of these compounds, HPLC was used to fractionate the mixture into monomers, dimers, and oligomers. Each fraction was analyzed for its effect on A $\beta$  conformational dynamics (circular dichroism), oligomerization (zero-length photochemical cross-linking), aggregation kinetics (Thioflavin T fluores-

cence), and morphology (electron microscopy). The relative activities of each fraction were determined on the basis of molar concentration (mol/L) or mass concentration (g/L). When molar concentration, the number concentration of each polyphenolic compound, was considered, the oligomer fraction was the most potent inhibitor of A $\beta$  oligomerization and aggregation. However, when mass concentration, the number concentration of phenolic groups, was considered, monomers were the most potent inhibitors. To understand these ostensibly contradictory results, a model of polyphenol:A $\beta$  complexation was developed. This model, which was found to be consistent with published X-ray crystallographic studies, offers an explanation for the effects of functional group polyvalency on inhibitor activity. Our data emphasize

Received July 2, 2015; accepted July 22, 2015.

Address correspondence and reprint requests to David B. Teplow, Department of Neurology, David Geffen School of Medicine, University of California, 635 Charles E. Young Dr. S, Room 445 Los Angeles, CA, 90095 USA. E-mail: dteplow@mednet.ucla.edu

<sup>1</sup>These authors contributed equally to this work.

<sup>2</sup>Present address: Department of Radiology, University of California, San Diego.

**Abbreviations used:** IC<sub>50</sub>, half-maximal inhibitory concentration; AD, Alzheimer's disease; APS, ammonium persulfate; A $\beta$ , amyloid  $\beta$ -protein; CD, circular dichroism; DTT, dithiothreitol; GSPE, grape seed polyphenolic extract; GST, glutathione S-transferase; HPLC, high-performance liquid chromatography; LMW, 'low molecular weight'; PICUP, photo-induced cross-linking of unmodified proteins; Ru(bpy), Tris(2,2'-bipyridyl)dichlororuthenium(II) hexahydrate; SC, statistical coil; TEM, transmission electron microscopy; ThT, Thioflavin T.

the importance of an in-depth understanding of the mechanism(s) underlying 'concentration dependence' in inhibitor systems involving polyfunctional agents.

Alzheimer's Disease (AD), the most common late-life neurodegenerative disorder, is estimated to affect > 35 million people worldwide, a number that is predicted to reach  $\approx$  115 million by 2050 (Brookmeyer *et al.* 2007). If therapies can be developed that delay disease onset and progression by just 1 year, there will be an estimated 9 million fewer AD cases by 2050 (Brookmeyer *et al.* 2007). Current AD treatments, which include blocking acetylcholine degradation or *N*-methyl-D-aspartate receptors, provide at best, modest, short-term symptomatic relief (Cummings 2004).

AD is characterized neuropathologically by the cerebral deposition of two hallmark proteinaceous aggregates—amyloid plaques, formed by the amyloid  $\beta$ -protein (A $\beta$ ), and neurofibrillary tangles, formed by the protein tau. Hardy and Higgins originally proposed the 'amyloid cascade hypothesis' of AD pathogenesis, wherein A $\beta$  fibrils are neurotoxic and lead to neuronal cell death (Hardy and Higgins 1992). However, subsequent biochemical, biological, and behavioral studies suggest that A $\beta$  oligomers may be the most important neurotoxic species (Klein 2006; Roychaudhuri *et al.* 2009). Blocking A $\beta$  assembly and neurotoxicity thus may be an attractive therapeutic approach.

Recent epidemiological data suggest that moderate consumption of red wine may prevent or delay the onset of AD (Letenneur *et al.* 1993; Dorozynski 1997; Orgogozo *et al.* 1997; Truelsen *et al.* 2002). Red wine contains a broad range of polyphenolic compounds that appear responsible for these protective effects. Polyphenols are plentiful in nature. Sources include berries, tea, beer, olive oil, chocolate/cocoa, coffee, walnuts, peanuts, pomegranates, popcorn, and yerba mate. Experimental evidence has shown that polyphenols are potent antioxidants, as well as inhibitors of A $\beta$  and tau self-assembly (Virgili and Contestabile 2000; Flamini 2003; Ono *et al.* 2008; Ho *et al.* 2009; Pasinetti *et al.* 2010). A commercially available grape seed polyphenolic extract (GSPE), MegaNatural-AZ<sup>®</sup> (Polyphenolics, Madera, CA, USA), significantly ameliorated AD-like neuropathology and cognitive deficits in the Tg2576 mouse model of AD (Wang *et al.* 2008). In the JNPL3 mouse model of tauopathy (containing the P301L mutation), oral administration of GSPE was observed to reduce oligomeric tau in the brain while also attenuating the severity of motor impairment typically observed (Pasinetti *et al.* 2010).

HPLC fractionation and mass spectrometry studies have confirmed that GSPE comprises polyphenols composed of catechin, epicatechin, and their derivatives (Fig. 1, Figure S1)

**Keywords:** Alzheimer's disease, amyloid  $\beta$ -protein (A $\beta$ ), grape seeds, inhibitors, oligomers, polyphenols. *J. Neurochem.* (2015) **135**, 416–430.

(Flamini 2003). Size-exclusion chromatography shows that GSPE is a mixture of monomers,<sup>1</sup> oligomers, and polymers (Wang *et al.* 2008, 2012; Sharma *et al.* 2011). Increasing numbers of monomer units of catechin and its derivatives combine to form GSPE oligomers as large as 10 monomers. Prior studies of GSPE activity have used unfractionated material (Ono *et al.* 2008). We sought here to determine the activities of pure monomers, dimers, and oligomers on A $\beta$  assembly. Analysis of the relative potencies of each fraction with respect to molar (M) and weight (g/L) concentration provided the information necessary for: (i) conception of a model explaining polyphenol:A $\beta$  interactions; and (ii) understanding how studies of multifunctional inhibitor compounds should be interpreted in the context of the development and use of GSPE for therapeutic purposes.

## Methods

### Chemicals and reagents

Chemicals were obtained from Sigma-Aldrich Co. (St. Louis, MO, USA) and were of the highest purity available. MegaNatural-AZ<sup>®</sup> comprises a mixture of polyphenolic compounds that has an average molecular weight of 580. High performance liquid chromatography (HPLC) produces fractions composed of compounds of average molecular weight 280, 560, and 2800, representing 8%, 75%, and 17%, respectively, of the total material (Wang *et al.* 2008; Pasinetti *et al.* 2010). For simplicity, we refer to these three fractions as 'monomer,' 'dimer,' and 'oligomer,' respectively, although each fraction is not a homogeneous population of molecules of a single molecular weight. Stock solutions of GSPE monomers, dimers, and GSPE mixture were solubilized at a concentration of 1 mM in 10 mM sodium phosphate buffer, pH 7.5. GSPE oligomers were first solubilized at 1 mM in 1% (v/v) ethanol in 10 mM sodium phosphate buffer, pH 7.5, and then diluted to 0.1% (v/v) ethanol in the same buffer.

### Preparation of A $\beta$

A $\beta$  was synthesized in the UCLA Biopolymer facility and then purified and characterized, as described previously (Walsh *et al.*

<sup>1</sup>The term 'monomer' refers to a single polyphenol-containing molecule, *not* to a single phenolic functional group. The simplest polyphenol is benzenediol (dihydroxybenzene), containing two hydroxyl groups. A typical monomer present in our GSPE preparation might contain 21 phenolic hydroxyl groups, thus a 1 M concentration of this monomer would be 21 M in phenol functional groups. Oligomers would contain proportionately higher numbers of phenolic groups. Further, 'monomer' comprises a variety of phenolic molecules with similar Stoke's radii.

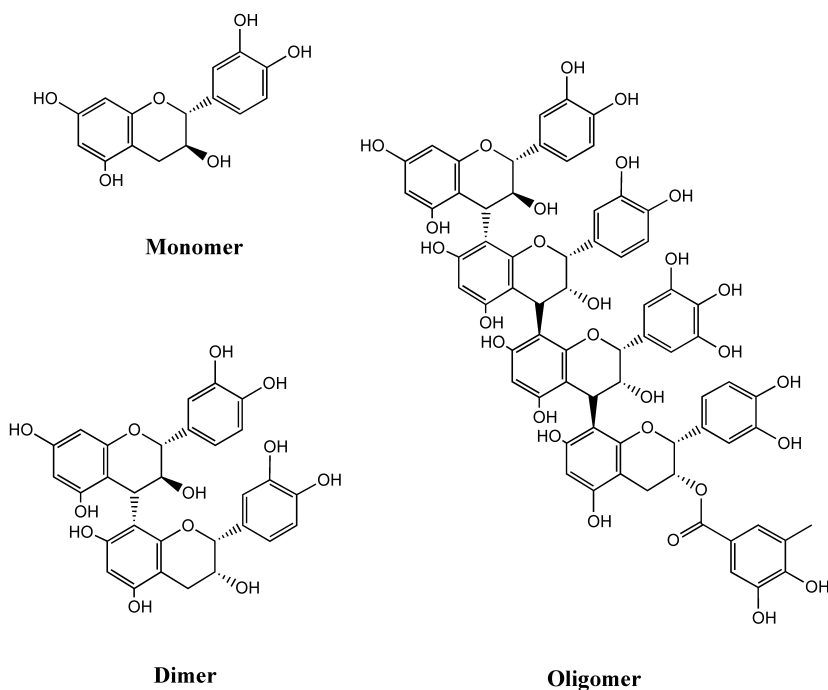


**Fig. 1** Structures of representative grape seed polyphenolic extract (GSPE) components. GSPE is a water-soluble polyphenolic extract from *Vitis vinifera* grape seeds. GSPE comprises catechin and epicatechins in monomeric (8%), dimeric (75%), and oligomeric (17%) forms. Examples of monomer, dimer, and oligomer structures are shown. The GSPE oligomer shown is composed of four monomer units: catechin, epicatechin, epigallocatechin, and epicatechin gallate. GSPE monomer, dimers, and oligomers likely are structurally heterogeneous.

1997). Briefly, peptide synthesis was performed on an automated peptide synthesizer (model 433A, Applied Biosystems, Foster City, CA, USA) using 9-fluorenylmethoxycarbonyl-based methods on preloaded Wang resins. Peptides were purified, using reverse-phase high-performance liquid chromatography (HPLC). Quantitative amino acid analysis and mass spectrometry yielded the expected compositions and molecular weights, respectively, for each peptide. Purified peptides were stored as lyophilizates at  $-20^{\circ}\text{C}$ . Peptides were prepared by dissolution in a 1 : 4.5 : 4 : 5 ratio of 60 mM NaOH:Milli-Q water:22.2 mM sodium phosphate, pH 7.5, to yield a nominal A $\beta$  concentration of 1 mg/mL in 10 mM sodium phosphate, pH 7.5. The peptide solution then was sonicated for 1 min in a bath sonicator (Branson Model 1510, Danbury, CT, USA) and filtered through a 30,000 molecular weight cut-off Microcon centrifugal filter device (Millipore, Billerica, MA, USA) for 15 min at 16 000 *g*. The eluate containing A $\beta$  was quantified through UV absorbance ( $\epsilon_{280} = 1280$  per cm/M), using a 1 cm quartz cuvette (Hellma, Plainview, NY, USA) and a Beckman DU-640 spectrophotometer (Beckman Instruments, Fullerton, CA, USA). All measurements were performed at  $22^{\circ}\text{C}$ . This protocol reproducibly yields aggregate-free A $\beta$  monomer in rapid equilibrium with low order oligomers, which is termed 'low molecular weight' A $\beta$  (Teplow 2006).

#### Photo-induced cross-linking of unmodified proteins (PICUP)

Immediately after preparation, 'low molecular weight' A $\beta$  solutions were diluted to 80  $\mu\text{M}$ , mixed with the GSPE fraction of interest (diluted to 16–72  $\mu\text{M}$ ), and cross-linked, using the PICUP method, as described (Bitan *et al.* 2001). Briefly, 1  $\mu\text{L}$  of 2 mM Tris(2,2'-bipyridyl)dichlororuthenium(II) hexahydrate (Ru(bpy)) and 1  $\mu\text{L}$  of 40 mM ammonium persulfate, each dissolved in water, were added to 18  $\mu\text{L}$  of protein solution. The final A $\beta$ :Ru(bpy): ammonium

persulfate molar ratios were 0.72 : 1 : 20. The mixture was irradiated for 1 s with a 'Fiber-Lite' high intensity visible light source (Dolan-Jenner, Boxborough, MA, USA) and the reaction then was immediately quenched with 1  $\mu\text{L}$  of 1 M dithiothreitol in water. SDS-PAGE and silver staining were used to determine the frequency distribution of A $\beta$  oligomers after incubation with GSPE. To do so, 21  $\mu\text{L}$  of each cross-linked sample was mixed with 21  $\mu\text{L}$  of 2  $\times$  sodium dodecyl sulfate sample buffer and then boiled for 10 min. Thereafter, 5  $\mu\text{L}$  of each sample was electrophoresed on a 10–20% gradient Tricine gel (Invitrogen, Carlsbad, CA, USA) and visualized by silver staining (SilverXpress, Invitrogen). Non-cross-linked samples were used as controls in each experiment. Glutathione S-transferase (GST) (Sigma-Aldrich) was used as a control for the PICUP chemistry (Ono *et al.* 2008). GST was dissolved in 10 mM sodium phosphate buffer, pH 7.4, at a concentration of 40  $\mu\text{M}$ . For PICUP, GST was diluted to 20  $\mu\text{M}$  in 10 mM phosphate buffer, pH 7.4, either alone or with 20  $\mu\text{M}$  of each GSPE fraction. PICUP then was performed as described above.

Silver-stained gels were scanned on a Canon CanoScan 9950 flatbed scanner. Images were converted into 256 grayscale and analyzed densitometrically by ImageJ 1.43r (<http://imagej.nih.gov/ij/>). Density profiles were determined by integration of the area under each peak, after baseline correction. Individual peak densities within a lane were then normalized to the total baseline-corrected peak area within that lane.

#### Circular dichroism spectroscopy (CD)

CD spectra of A $\beta$  alone, or of A $\beta$  with equimolar GSPE fractions, were acquired immediately after sample preparation or following 1, 2, 3, 4, 7, or 8 days of incubation. Forty  $\mu\text{M}$  A $\beta$ 40 was incubated in 1 mm path length quartz cuvettes (Hellma, Forest Hills, NY, USA) at  $22^{\circ}\text{C}$  with constant end-over-end rotation (Appropriate Technical

Resources, Laurel, MD, USA). Twenty-five  $\mu\text{M}$  A $\beta$ 42 also was incubated in 1 mm path length quartz cuvettes, but at 37°C and without rotation. CD spectra were acquired with a J-810 spectropolarimeter (JASCO, Tokyo, Japan). Following temperature equilibration, spectra were recorded at 22°C from 195 to 260 nm at 0.2 nm resolution with a scan rate of 100 nm/min. Ten scans were acquired and averaged for each sample. Buffer spectra, or spectra of the relevant GSPE fraction in buffer, were subtracted from experimental spectra prior to data analysis. We note that only the GSPE oligomer fraction produced a spectrum with significant intensity, especially below 200 nm.

### Thioflavin T fluorescence

A $\beta$  mixed with each GSPE fraction was incubated at 37°C in 96-well microtiter plates (Thermo Scientific, Rochester, NY, USA) with 250 rpm orbital shaking. This method produced accelerated fibril formation without an observable lag phase. ThT fluorescence measurements were acquired with a Synergy HT fluorometer (BioTek, Beijing, China) with an excitation wavelength of 420 nm and an emission wavelength of 485 nm, each with 10 nm slit widths. ThT ( $2 \times$  A $\beta$  concentration) fluorescence intensities were measured immediately after sample preparation and periodically for up to 1 month thereafter. To ensure that the GSPE fractions did not interfere with the ThT measurements, optical absorption of each GSPE fraction was measured. No significant absorption was observed above 250 nm.

A $\beta$ 40 (20  $\mu\text{M}$ ) was incubated with GSPE fractions of 4.8–200  $\mu\text{M}$  concentration. Experiments were done in triplicate or higher replication number, except at the highest concentrations tested for GSPE mixture (77 and 96  $\mu\text{M}$ ), oligomer (16  $\mu\text{M}$ ), dimer (80 and 100  $\mu\text{M}$ ), and monomer (160 and 200  $\mu\text{M}$ ), where one replicate made clear the trend of nearly complete inhibition. A $\beta$ 42 (10  $\mu\text{M}$ ) was incubated with GSPE fractions of 0.48–100  $\mu\text{M}$  concentration.

GraphPad Prism was used for graphing and analysis of the ThT fluorescence data. At the lowest GSPE concentrations examined (4.8  $\mu\text{M}$  for A $\beta$ 40 and 0.48  $\mu\text{M}$  for A $\beta$ 42), we observed ThT intensities of  $\sim 45\%$  (A $\beta$ 40) and  $\sim 65\%$  (A $\beta$ 42) of the control intensity, indicating inhibition even at these low concentrations. The half-maximal inhibitory concentration (IC<sub>50</sub>) for each GSPE fraction was determined, using the general form of the four parameter logistic IC<sub>50</sub> equation  $y = \min + \{(max - \min)/(1 + [(\log(\text{IC}_{50})/x)^h])\}$ ; where  $y$  is the normalized fluorescence intensity (%),  $\min$  is the lowest normalized fluorescence intensity observed (%),  $\max$  is set to 100%,  $x$  is log (GSPE concentration [in  $\mu\text{M}$ ]), and the Hill slope parameter  $h$  was set to  $-1$ , indicating a downward trajectory (Turner and Charlton 2005).

### Transmission electron microscopy (TEM)

Ten  $\mu\text{L}$  of A $\beta$ 40 (20  $\mu\text{M}$ ) or A $\beta$ 42 (10  $\mu\text{M}$ ), with or without equimolar GSPE, was spotted onto a carbon-coated Formvar grid (Electron Microscopy Sciences, Hatfield, PA, USA) and incubated for 2 min. The droplet then was displaced with an equal volume of 1% (w/v) filtered (0.2  $\mu\text{M}$ ) uranyl acetate in water (Electron Microscopy Sciences). This solution was wicked off and then the grid was air dried. Samples were examined in an operator-blinded fashion, using a JEOL 1200 EX transmission electron microscope with an accelerating voltage of 80 kV. Digital images were

analyzed with ImageJ 1.43r, using the ‘measure tool’ to calculate dimensions.

## Modeling of interactions between GSPE and A $\beta$ aggregates

### Three-dimensional construction of GSPE (monomer, dimer and oligomer) models

The 3D structural model of GSPE monomer (catechin) is from the ZINC database (entry: 119983) (<http://zinc.docking.org/>) and from the Chemical Database Service (Fletcher *et al.* 1996). We built the GSPE dimer and oligomer with Weblab Viewer Pro (Accelrys, San Diego, CA, USA), based on the structure of GSPE monomer. Additional polyphenol moieties (epicatechin, epigallocatechin, and epicatechin gallate) and all hydrogen atoms were added according to the chemical structures of GSPE dimer and oligomer, respectively (Figure S1). The configuration at the chiral center of each model was carefully inspected and corrected. Finally, the entire GSPE dimer and oligomer structures were iteratively minimized using the ‘Clean’ feature of Weblab Viewer Pro.

### Modeling interactions

A partially folded A $\beta$ 40 structure derived using solution-state NMR (Vivekanandan *et al.* 2011) (PDB entry: 2LFM) was used to model A $\beta$  interactions with the catechin monomer, dimer, and oligomer. SwissDock is a tool that can search for possible protein and small molecule interactions (Gazova *et al.* 2013; Kumar *et al.* 2013). Here, SwissDock (Grosdidier *et al.* 2011a,b) was used to predict possible molecular interactions between A $\beta$ 40 and GSPE monomers or dimers. SwissDock parameters included: (i) the region of interest was not defined; (ii) the docking type was set to ‘accurate;’ and (iii) flexibility was allowed for side chains within 3 Å of any atom of the ligand in its reference-binding mode. SwissDock could not successfully dock the GSPE oligomer to A $\beta$ . Therefore, for illustrative purposes only, we manually positioned the GSPE oligomer on the A $\beta$  structure.

### Computational docking of GSPE onto the A $\beta$ fibril model

We used an A $\beta$  fibrillar structure from a solid-state NMR fibril model of full-length A $\beta$  (PDB entry: 2LMO) (Petkova *et al.* 2006). Each GSPE molecule was prepared for Rosetta docking simulations, as described previously (Jiang *et al.* 2013). The ensemble of ligand internal conformations near the starting conformation of each molecule was built by perturbing a small deviation ( $\pm 5^\circ$ ) of torsion angle for each rotatable bond of the ligand. Approximately 100 conformations for each ligand were generated and made available for the Rosetta docking simulation. We used a modified Rosetta Ligand Dock algorithm with near-‘native’ perturbation sampling for both protein side-chain conformations and ligand internal conformations (Jiang *et al.* 2013). Each GSPE molecule (monomer, dimer, or oligomer) was docked onto the A $\beta$  fibrillar structure with 1000 docking simulations. The final docked models were selected based on the largest predicted binding energy (Meiler and Baker 2006; Davis and Baker 2009) and best shape complementarity (Lawrence and Colman 1993). The predicted binding energy and physically meaningful energy terms (Lennard–Jones interactions, solvation, hydrogen bonding, and electrostatics) of the selected models are compared in Table S1.

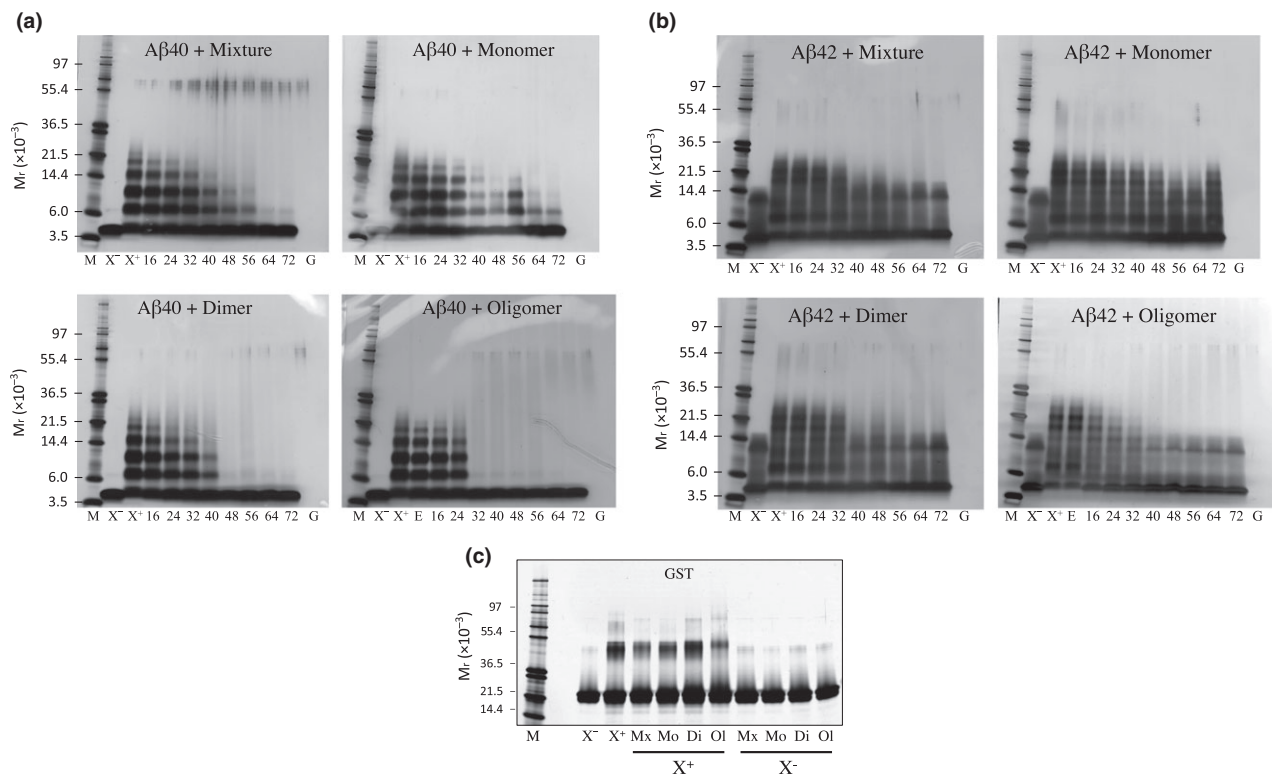


**Fig. 2** Oligomerization of A $\beta$  in the presence of grape seed polyphenolic extract (GSPE). Photo-induced cross-linking of unmodified proteins (PICUP), sodium dodecyl sulfate–polyacrylamide gel electrophoresis (SDS–PAGE), and silver staining were used to determine the oligomer size distributions of (a) A $\beta$ 40 and (b) A $\beta$ 42 with varying concentrations of GSPE mixture, monomer, dimer, or oligomer, as indicated. Lane abbreviations

are: M, MW markers; X<sup>-</sup>, non-cross-linked A $\beta$ ; X<sup>+</sup>, cross-linked A $\beta$ ; E, cross-linked A $\beta$  with 0.1% (v/v) ethanol; A $\beta$ 40 cross-linked with 16, 24, 32, 40, 48, 56, 64, and 72  $\mu$ M GSPE, respectively; cross-linked GSPE alone, 72  $\mu$ M. (c) Glutathione S-transferase (GST) was used as a positive control for cross-linking. GST was mixed with equimolar GSPE mixture, monomer, dimer, or oligomer and then either was cross-linked or not cross-linked.

## Results and discussion

Thousands of polyphenolic compounds are found in wine, including flavonoids and non-flavonoids. Flavanoids, which include anthocyanidins and tannins, contribute to the color and taste of wine. Non-flavonoids include resveratrol and compounds that impart acidity, including benzoic, caffeic, and cinnamic acid. GSPE is a polyphenolic extract derived from *Vitis vinifera* grape seeds that comprises catechin, epicatechin, and their derivatives (including epigallocatechin and epicatechin gallate) (Pasinetti *et al.* 2010). GSPE has been shown to reduce AD-like cognitive decline and high molecular weight cerebral amyloid deposition in Tg2576 mice, as well as protect differentiated PC12 cells *in vitro* from A $\beta$ -induced injury (Ono *et al.* 2008). GSPE blocks the statistical coil (SC)  $\rightarrow$   $\alpha$ -helix/ $\beta$ -sheet secondary structure transitions that are typical of A $\beta$  self-assembly (Kirkitadze *et al.* 2001) and blocks A $\beta$  oligomerization, protofibril formation, and fibril formation (Ono *et al.* 2008). However, size–activity relationships on specific components of the GSPE mixture have not been done. For this reason, we studied here the effects of three components of the GSPE

mixture on A $\beta$  assembly—monomers, dimers, and oligomers.

### Effects of GSPE on A $\beta$ oligomerization

We used photo-induced cross-linking of unmodified proteins (PICUP), a zero-length chemical cross-linking method (Teplow *et al.* 2006), combined with sodium dodecyl sulfate–polyacrylamide gel electrophoresis (SDS–PAGE) and silver staining, to evaluate the effect of GSPE on A $\beta$  oligomerization. Non-cross-linked A $\beta$ 40 was monomeric (Fig. 2a, X<sup>-</sup>), whereas cross-linked A $\beta$ 40 displayed an oligomer distribution comprising predominantly monomers through tetramers, along with some larger oligomers (Fig. 2a, X<sup>+</sup>). All three GSPE components inhibited A $\beta$ 40 oligomerization in a concentration-dependent manner. The mixture, dimers, and oligomers were capable of inhibiting A $\beta$ 40 oligomerization essentially completely at concentrations < 64  $\mu$ M, < 48  $\mu$ M, and < 32  $\mu$ M, respectively. For all fractions tested, the amount of A $\beta$ 40 monomer showed a concentration-dependent increase as GSPE concentration increased, as would be expected if the GSPE blocked monomer self-association or caused aggregate dissociation.

**Table 1** Effect of grape seed polyphenolic extract (GSPE) on A $\beta$ 40 oligomerization

A $\beta$ 40 oligomer	GSPE fraction IC <sub>50</sub> ( $\mu$ M)			
	Mixture	Monomer	Dimer	Oligomer
Dimer	49	48	40	27
Trimer	40	40	34	26
Tetramer	33	36	34	23
Pentamer	41	26	34	26
Hexamer	8	8	16	7

IC<sub>50</sub> values are reported for A $\beta$ 40 dimer through hexamer for each GSPE fraction tested. Values were determined by densitometry of cross-linked oligomer bands on silver-stained gels.

We note that for the GSPE oligomer only, 0.1% (v/v) ethanol was used to facilitate dissolution. For this reason, we determined if 0.1% ethanol by itself altered A $\beta$  oligomerization. No effects were observed for either A $\beta$ 40 (Fig. 2a and e) or A $\beta$ 42 (Fig. 2b and e). We also note the presence of material with an  $M_r \approx 58$  kDa, which likely corresponds to keratin, an oft observed contaminant in SDS-PAGE (Ochs 1983). Densitometric analysis of the silver-stained gels for each A $\beta$ 40-GSPE combination allowed calculation of IC<sub>50</sub> values (Table 1). For A $\beta$ 40, GSPE oligomer was the most potent oligomerization inhibitor.

Non-cross-linked A $\beta$ 42 displayed monomer and trimer bands (Fig. 2b, X<sup>-</sup>). The A $\beta$ 42 trimer band is a sodium dodecyl sulfate-induced artifact (Bitan *et al.* 2003). Cross-linked A $\beta$ 42 produced an oligomer distribution comprising monomers through octamers, with nodes at monomer, dimer, and pentamer/hexamer (Fig. 2b, X<sup>+</sup>). As with A $\beta$ 40, GSPE preparations produced concentration-dependent decreases in oligomerization. For all GSPE fractions, with the exception of GSPE monomer, concentrations < 40  $\mu$ M demonstrated essentially complete inhibition of A $\beta$ 42 oligomerization. With GSPE monomer, concentration-dependent inhibition of oligomerization was observed, but even at the highest monomer concentrations, the inhibition was incomplete. A $\beta$ 42 monomer and trimer bands showed a GSPE concentration-dependent increase in staining intensity in all samples, as would be expected because monomer and trimer are characteristic of non-cross-linked A $\beta$ 42 and indicate no oligomerization. Interestingly, the tetramer band intensities remained relatively consistent regardless of GSPE concentration. Determination of IC<sub>50</sub> values (Table 2) revealed that oligomer was the most potent GSPE fraction, as was observed for A $\beta$ 40.

In theory, the inhibition of A $\beta$  oligomerization could be an artifact resulting from GSPE interfering with the PICUP chemistry. To rule out this possibility, we studied the cross-linking of glutathione S-transferase (GST), a 26 kDa protein that has been used in the past as a positive control for the

**Table 2** Effect of grape seed polyphenolic extract (GSPE) on A $\beta$ 42 oligomerization

A $\beta$ 42 oligomer	GSPE fraction IC <sub>50</sub> ( $\mu$ M)			
	Mixture	Monomer	Dimer	Oligomer
Dimer	44	–	35	21
Pentamer	32	45	38	35
Hexamer	32	40	33	27
Heptamer	24	30	22	24
Octamer	19	20	9	17

IC<sub>50</sub> values are reported for A $\beta$ 42 dimer, and for pentamer through octamer, for each GSPE fraction tested. (See text regarding omission of trimer and tetramer.) Values were determined by densitometry of cross-linked oligomer bands on silver-stained gels.

PICUP chemistry (Fig. 2c) (Fancy and Kodadek 1999). Non-cross-linked GST exhibited predominantly monomers, with some dimers. Cross-linking produced monomer and dimer bands, along with faint trimer and tetramer bands. No qualitative changes in GST cross-linking were observed in the presence of GSPE mixture, monomer, dimer, or oligomer when tested at a GSPE:protein ratio of 1 : 1 at 20  $\mu$ M. Slightly more GST trimer and tetramer are observed when cross-linked in the presence of GSPE oligomer. GST:GSPE mixtures also were examined without cross-linking, and each displayed predominantly monomers and some dimers, similar to what was observed with GST alone. These results show that the GSPE did not have a significant effect on the PICUP chemistry.

Taken together, the data show: (i) the GSPE mixture and each fraction (monomer, dimer, and oligomer) are potent inhibitors of A $\beta$ 40 and A $\beta$ 42 oligomerization; (ii) the oligomeric form of GSPE was the most potent inhibitor of A $\beta$  oligomerization (lowest IC<sub>50</sub>); and (iii) except for effects against A $\beta$ 40 pentamer and hexamer, the monomeric form of GSPE was least potent. We also note that if inhibition of oligomerization was incomplete, i.e., if low-order oligomers, and not just monomers, were present, larger assemblies formed upon incubation (Fig. 6).

### A $\beta$ secondary structure dynamics

To monitor secondary structure during peptide assembly, circular dichroism spectroscopy (CD) was performed. In the absence of GSPE (Fig. 3a and b, 'A $\beta$  alone'), A $\beta$ 40 and A $\beta$ 42 initially displayed high statistical coil (SC) content, which was apparent from a prominent minimum between 195 and 200 nm and a monotonic increase in molar ellipticity as wavelength increased. A transition to mixed  $\alpha/\beta$  conformation was observed after 1 day of incubation. This spectrum changed thereafter into one typical of  $\beta$ -sheet conformation, namely with a single minimum at  $\approx 214$  nm and a maximum below 200 nm. In contrast, when A $\beta$ 40

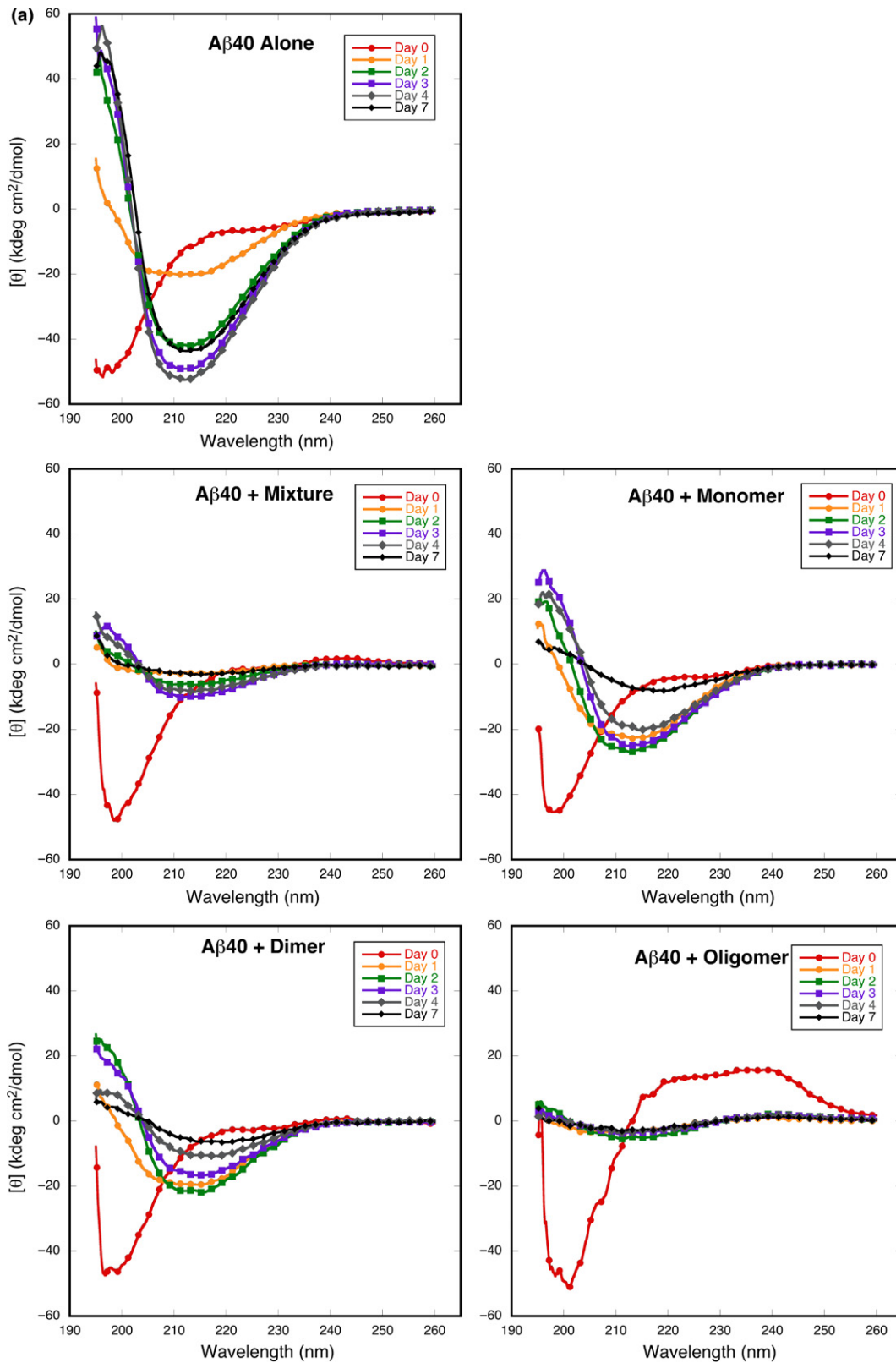


**Fig. 3** Effect of grape seed polyphenolic extract (GSPE) on the evolution of Aβ secondary structure. Circular dichroism (CD) spectra of (a) Aβ40 and (b) Aβ42 incubated at 22°C with or without equimolar

GSPE fractions and monitored at days 0 (red circle), 1 (orange circle), 2 (green square), 3 (purple square), 4 (gray diamond), and 7 (black diamond).



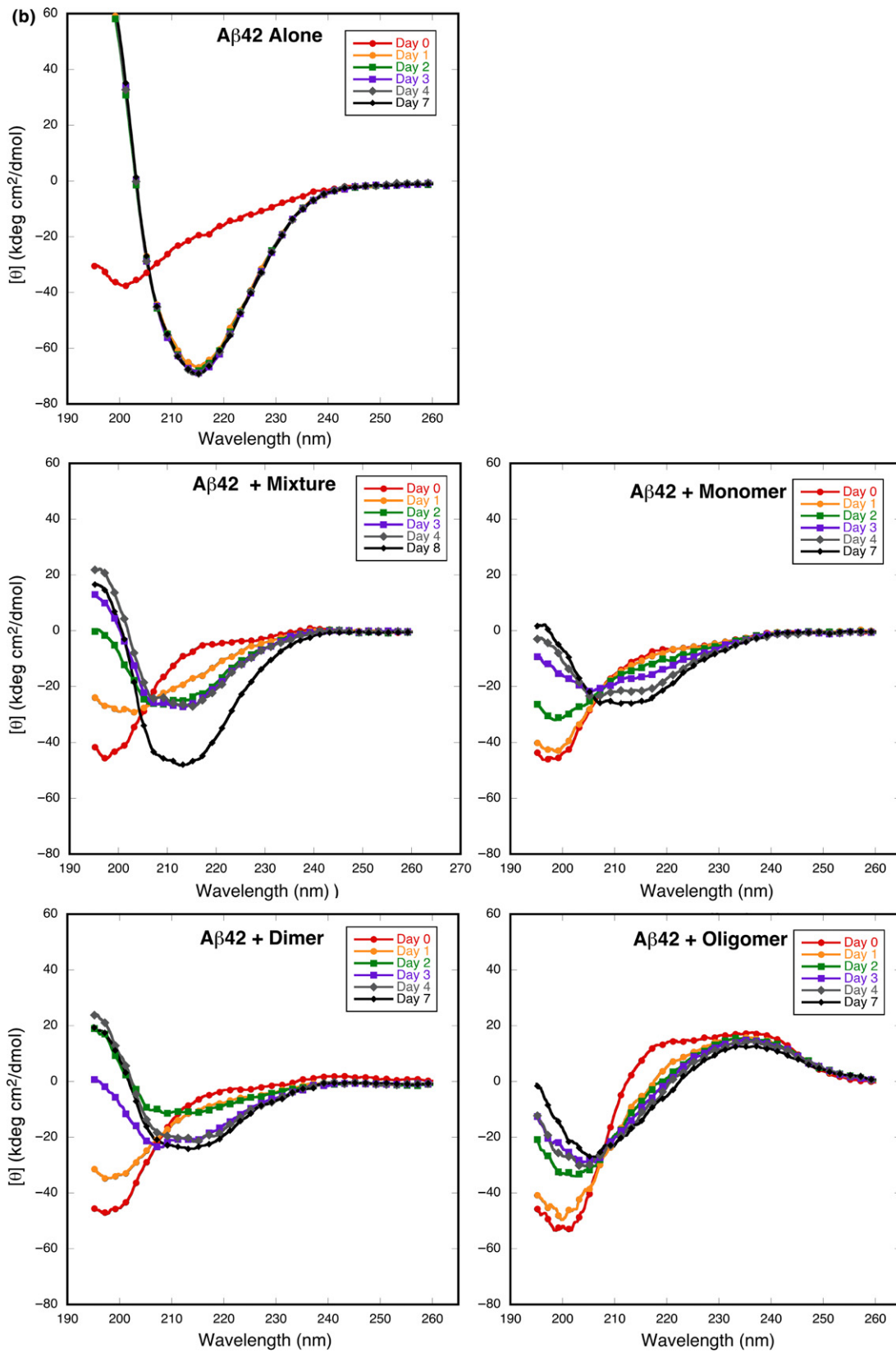


Fig. 3 Continued.

was treated with an equimolar amount of each GSPE fraction, the evolution of secondary structure did not occur in the same manner. Instead, mixed  $\alpha/\beta$  structure was observed prior to the development of  $\beta$ -sheet and this structure remained until longer incubation times (e.g., see GSPE dimer at day 3 and GSPE monomer at day 4) (Fig. 3a). The magnitude of the CD signal for incubations with the mixture and oligomer GSPE decreased compared to the spectrum without GSPE, suggesting a decreased amount of protein in solution. Nevertheless, the spectra were interpretable, yielding the observation that, for each condition, the protein-GSPE mixtures displayed spectra consistent with varying amounts of  $\alpha$ -helix and  $\beta$ -sheet secondary structure.

For A $\beta$ 42, each of the GSPE fractions inhibited SC  $\rightarrow$   $\alpha/\beta$  transitions (Fig. 3b). By day 1, A $\beta$ 42 alone displayed a clear  $\beta$ -sheet spectrum with a minimum at 215 nm and a maximum at  $<$  195 nm, whereas in equimolar A $\beta$ 42:GSPE mixtures, each sample displayed nearly the same amount of SC signal intensity as seen initially. By 7 or 8 days, the spectra of A $\beta$ 42 incubated with GSPE mixture, dimer, or monomer remained constant. Inspection of these spectra indicated the formation of A $\beta$  conformers containing both  $\alpha$ -helical (minimum at  $\approx$ 208 nm) and  $\beta$ -sheet (minimum at  $\approx$  214 nm) secondary structure. For A $\beta$ 42 incubated with GSPE oligomer, the spectrum at day 7 displayed a minimum at higher wavelengths compared to the initial spectrum with a minimum at 200 nm, suggesting an increase in *non-SC* structure.

GSPE and each of its component fractions thus prevented the SC  $\rightarrow$   $\beta$ -sheet structural transition occurring during fibril formation. Preventing this transition could be beneficial clinically, assuming that any A $\beta$  assemblies remaining were non-toxic. If one argues that the same biophysical effects observed *in vitro* occur *in vivo*, then the beneficial effects of GSPE administration observed in Tg2576 animals support a therapeutic mechanism involving A $\beta$  assembly inhibition (Wang *et al.* 2008).

#### Time dependence of ThT fluorescence

Thioflavin T (ThT) fluorescence was used to monitor  $\beta$ -sheet formation, a proxy for fibril formation (Groenning 2010). A $\beta$ 40 and A $\beta$ 42 displayed an initial increase in fluorescence intensity that rose monotonically before leveling off (Fig. 4a and b). Incubation of 20  $\mu$ M A $\beta$ 40 with equimolar amounts of GSPE reduced ThT intensity, indicating inhibition of  $\beta$ -sheet formation (Fig. 4a). Monomeric GSPE caused a substantial decrease in the initial rate of increase in fluorescence and in the final intensity of ThT fluorescence. Oligomeric GSPE caused the greatest decreases, whereas the mixture and dimeric GSPE fractions had intermediate effects. An identical rank order of GSPE effects was observed in studies on A $\beta$ 42 (Fig. 4b), namely oligomer  $>$  dimer  $\approx$  mixture  $>$  monomer. However, the

rates of increase in ThT fluorescence were  $\sim$  3-fold greater than those in the A $\beta$ 40 system.<sup>2</sup>

#### Concentration-dependence of GSPE effects on ThT fluorescence of A $\beta$

The polyphenolic A $\beta$  assembly inhibitors are, in at least one respect, a unique class of compounds because the chemical groups thought responsible for their activity, the phenolic hydroxyls, are present in significantly greater numbers than are the compounds themselves, i.e., the molar ratio of phenolic hydroxyls/polyphenol compound  $\gg$  1. The average MW of the monomer GSPE fraction is 10-fold less than the average MW of the oligomer fraction (280 vs. 2800), suggesting that the oligomers are formed by approximately 10 monomer subunits and thus contain 10-fold greater numbers of phenolic hydroxyls. This logic suggests that determination of inhibitory activity must consider not only molar concentration-dependence (mol/L), but number concentration of phenolic functionalities, which is proportional to mass concentration (g/L). However, studies of the 'concentration-dependence' of A $\beta$  assembly inhibitors most often use mono-functional inhibitors and a molar concentration (mol/L) metric (Ono *et al.* 2008; Sinha *et al.* 2011; Orlando *et al.* 2012).

Here, to elucidate the effects of size and functional group number on inhibitory activity, we determined the relative activities of each fraction as a function of molar concentration (mol/L) and mass concentration (g/L). The first method revealed activity in terms of number concentration of each polyphenolic compound, but did not address the question of total number of phenolic functional groups present or their structural arrangement. The second method revealed activity in terms of number concentration of phenolic groups, but not concentration of each compound on which the phenolic groups were present. Distinguishing the effects of these two variables is critical for understanding the mechanism of action of the polyphenolic inhibitors (see note 1).

To determine the *molar* concentration-dependence of GSPE inhibition of A $\beta$  ThT fluorescence, we assayed GSPE fractions at concentrations of 0.1–100  $\mu$ M, keeping the concentrations of A $\beta$ 40 and A $\beta$ 42 constant at 20 and 10  $\mu$ M, respectively. The results are summarized in Fig. 5, in which we have plotted GSPE concentration versus the percent maximal fluorescence intensity that A $\beta$ 40 (Fig 5a) or A $\beta$ 42 (Fig. 5b) reached in its plateau phase. All data sets were fit to a four parameter logistic equation to derive relative half-

<sup>2</sup>Based on the orthogonal data showing the inhibition of fibril formation by CD and transmission electron microscopy (TEM) (see TEM section and Fig. 6), and the ThT concentration dependence data described below, we are confident that the decrease in ThT signal indicates fewer amyloid fibrils—not merely an artefactual decrease due to GSPE interacting with the fluorophore.

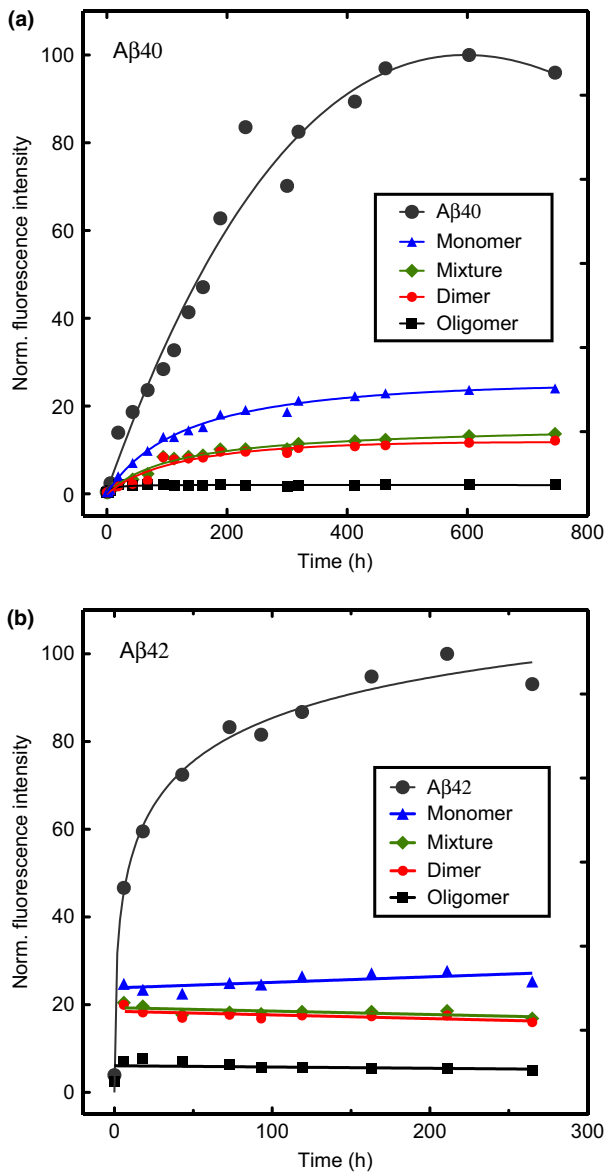


**Fig. 4** Effect of grape seed polyphenolic extract (GSPE) fractions on the evolution of Thioflavin T (ThT) fluorescence from A $\beta$ . ThT fluorescence intensities were measured for (a) A $\beta$ 40 and (b) A $\beta$ 42 incubated alone or with GSPE fractions. Fluorescence intensities were normalized to the highest value for each experimental condition. Data shown are representative of each of four replicates for A $\beta$ 40 and 5 replicates for A $\beta$ 42.

maximal inhibitory concentration (IC<sub>50</sub>) values for each GSPE fraction (See Thioflavin T fluorescence in Materials and Methods).

Oligomeric GSPE had the lowest IC<sub>50</sub> value, 0.87  $\mu$ M, with A $\beta$ 40, whereas monomeric GSPE had the highest value (5.3  $\mu$ M) (Table 3). The GSPE mixture and dimer samples displayed intermediate IC<sub>50</sub> values of 3.2 and 2.6  $\mu$ M, respectively. These IC<sub>50</sub> values are consistent with the rank

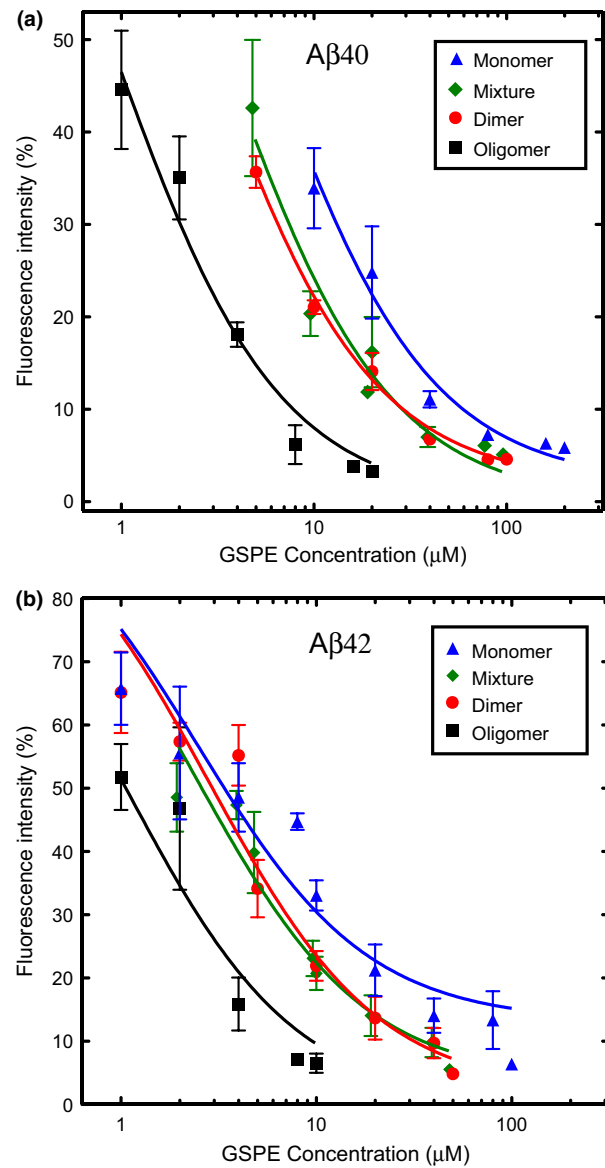


**Fig. 5** Concentration-dependence of inhibition of A $\beta$  Thioflavin T (ThT) fluorescence by grape seed polyphenolic extract (GSPE). (a) A $\beta$ 40 and (b) A $\beta$ 42 were incubated with varying concentrations of GSPE mixture, oligomer, dimer, or monomer. Final ThT fluorescence intensities were measured for each sample and normalized to the corresponding A $\beta$ 40 or A $\beta$ 42 alone. The data herein were used to derive IC<sub>50</sub> values (Table 3).

order of inhibition of oligomerization observed in our PICUP experiments. For A $\beta$ 42, as for A $\beta$ 40, oligomeric GSPE had the lowest IC<sub>50</sub>. GSPE mixture, monomer, and dimer displayed similar IC<sub>50</sub> values (2.4–2.8  $\mu$ M; Table 3). These values were of the same order of magnitude as observed with A $\beta$ 40, with the notable exception that GSPE monomer was approximately twice as effective an inhibitor of A $\beta$ 42 oligomerization, on a molar basis, than of A $\beta$ 40 oligomerization.

**Table 3** Effect of grape seed polyphenolic extract (GSPE) on A $\beta$  aggregation

Peptide	Mixture	Monomer	Dimer	Oligomer
A $\beta$ 40	3.2 (2.1-4.8)	5.3 (3.1-8.8)	2.6 (2.1-3.3)	0.87 (0.63-1.2)
A $\beta$ 42	2.4 (1.7-3.3)	2.5 (1.7-3.6)	2.8 (2.1-3.8)	1.1 (0.68-1.7)

IC<sub>50</sub> values ( $\mu$ M) are reported for A $\beta$ 40 (20  $\mu$ M) and A $\beta$ 42 (10  $\mu$ M) for each GSPE fraction tested. Values were determined by analysis of the ThT concentration-response curves for each condition at the final time-point measured. 95% confidence intervals are indicated in parentheses.

**Table 4** Effect of grape seed polyphenolic extract (GSPE) on A $\beta$  aggregation

Peptide	Mixture	Monomer	Dimer	Oligomer
A $\beta$ 40	1.9	1.5	1.5	2.4
A $\beta$ 42	1.4	0.7	1.6	3.1

IC<sub>50</sub> values in ng/L are reported for A $\beta$ 40 (20  $\mu$ M) and A $\beta$ 42 (10  $\mu$ M) for each GSPE fraction tested. Values were derived by converting the IC<sub>50</sub> in  $\mu$ M from Table 3 into ng/L using the average MW determined for each GSPE fraction.

To determine the mass concentration-dependence of GSPE inhibition of A $\beta$  ThT fluorescence, we determined the IC<sub>50</sub> values in units of ng/L (Table 4). Interestingly, this method of analysis of A $\beta$ 40 inhibition revealed that monomer and dimer were most inhibitory, whereas oligomer was least inhibitory, a result opposite to that observed considering inhibitor molarity (Table 3). For A $\beta$ 42, monomer also was the most effective inhibitor and oligomer was the least

effective. We note that the monomer IC<sub>50</sub> (0.7 ng/L) was significantly lower than in the A $\beta$ 40 system (1.5 ng/L) and was the lowest IC<sub>50</sub> among all eight samples. Dimer and mixture samples showed mid-range IC<sub>50</sub> values that were very similar (1.6 vs. 1.4 ng/L, respectively).

### Assembly morphology

To determine the morphology of structures formed in the presence or absence of GSPE, TEM was performed after 14 days incubation at 37°C. Straight and curved filaments were observed in untreated A $\beta$ 40 and A $\beta$ 42 (Fig. 6). These data were consistent with the strong  $\beta$ -strand content of the CD spectra observed at day 7 (Fig. 3a and b, A $\beta$  Alone).

A $\beta$ 40 displayed globular structures ranging from 7 to 20 nm in diameter (presumably representing oligomers) and fibrils with widths ranging from 10 to 15 nm and lengths up to 1  $\mu$ m (Fig. 6). When A $\beta$ 40 was treated with equimolar GSPE and its fractions, significantly fewer fibrils were observed. In A $\beta$ 40 samples treated with GSPE mixture, monomer, dimer, and oligomer fractions, globular structures were observed with diameters from 7 to 30 nm. These globular structures most frequently had diameters  $\approx$  20 nm.

A $\beta$ 42 displayed mostly fibrils, with widths of  $9.5 \pm 0.8$  nm and lengths exceeding 2.6  $\mu$ m, and globular structures ranging from 7 to 30 nm in diameter (average diameter  $\approx$  20 nm) (Fig. 6). Compared to A $\beta$ 42 alone, A $\beta$ 42 treated with GSPE mixture and each fraction showed an overall decrease in the amount of fibrils observed and an increase in the amount of globular assemblies ranging from 7 to 30 nm. The average width and morphology of A $\beta$ 42 fibrils did not change significantly in the presence of GSPE,

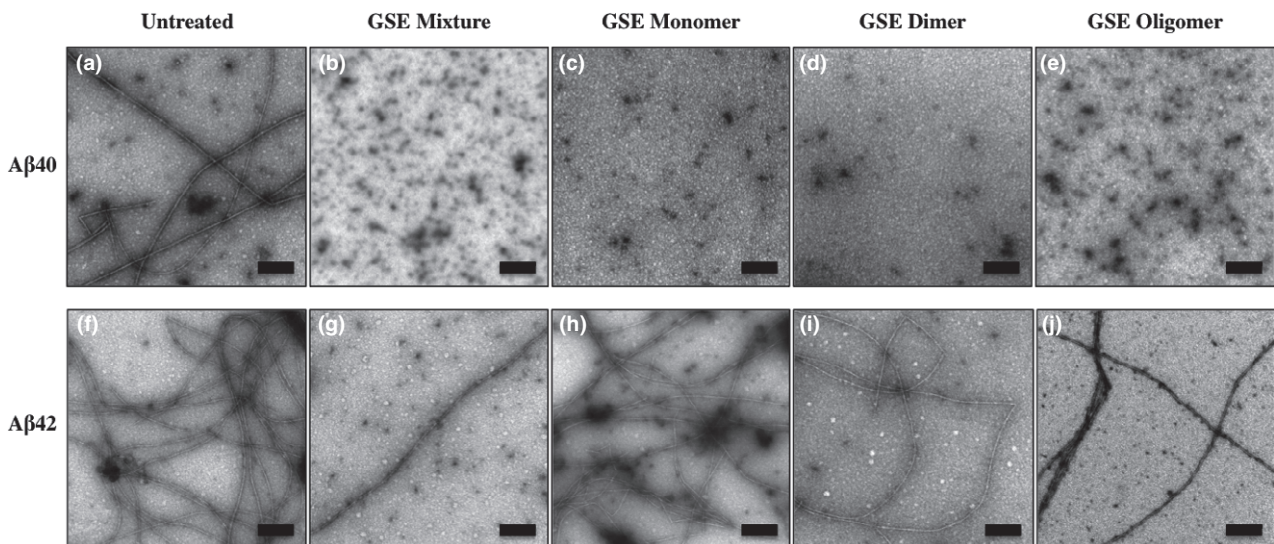


**Fig. 6** Electron microscopy of A $\beta$ 40 and A $\beta$ 42 with and without equimolar grape seed polyphenolic extract (GSPE) mixture, oligomer, dimer, or monomer. Transmission electron microscopy (TEM) was performed after 14 days of incubation at 37°C. Amyloid fibrils are observed for A $\beta$ 40 and

A $\beta$ 42 alone. In the presence of GSPE mixture, monomer, dimer, or oligomer, A $\beta$ 40 displayed globular structures, whereas A $\beta$ 42 displayed fibrils and small globular and amorphous assemblies. Panels shown are representative of the entire sample. Scale bar: 200 nm.

though the density of fibrils was noticeably diminished in the presence of GSPE mixture, dimer, and oligomer. All GSPE fractions also caused increases in the number of amorphous assemblies, both for A $\beta$ 42 and for A $\beta$ 40 (data not shown).

#### A model of the action of GSPE components on A $\beta$ assembly

The PICUP, ThT, and TEM data all show that both oligomer and fibril formation were inhibited by each GSPE fraction. GSPE appears to be a more potent inhibitor of A $\beta$ 40 fibril formation than of A $\beta$ 42 fibril formation. When the relative inhibitory potency of the different GSPE fractions is determined based upon *equivalent masses* (g/L), a rank order of monomer > dimer  $\approx$  mixture > oligomer is observed. In contrast, the opposite rank order is observed when *equivalent concentrations* (M) of each fraction are considered. How can this apparent conundrum be explained? We cannot be sure, but we offer a reasonable hypothesis.

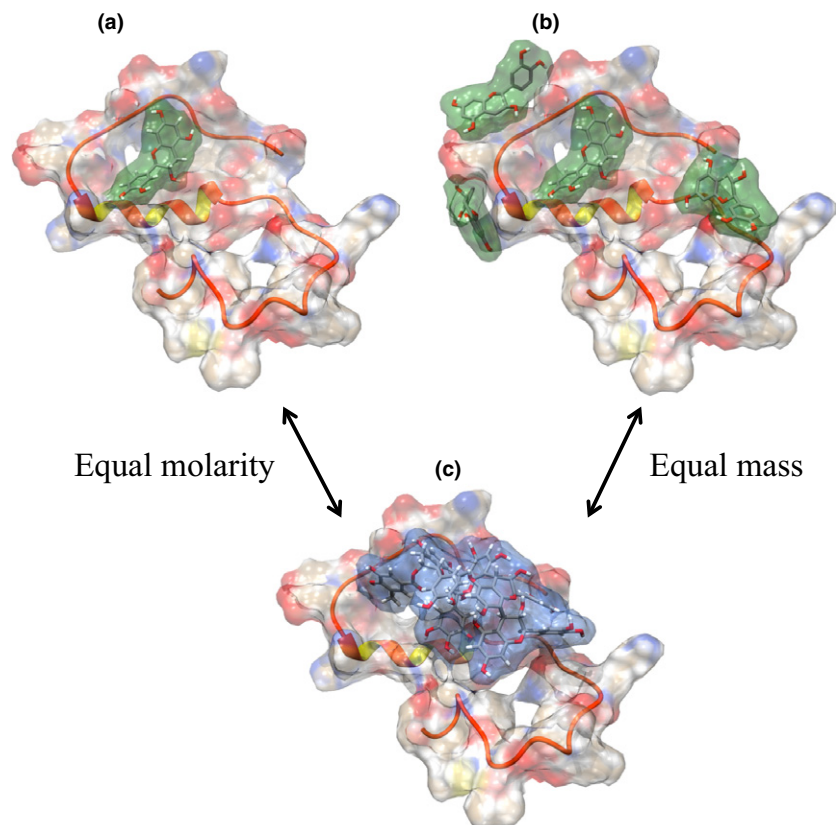
One set of our experiments compared *equimolar* concentrations of each GSPE fraction. If we consider only oligomer and monomer for the moment, this means that at any given concentration, the mass (g/L) of oligomer used was 10-fold greater than that of monomer. In addition, if we estimate an average of 5.5 OH groups per unit weight — the average number on catechin, epicatechin, epigallocatechin, and epicatechin gallate — then the oligomer prepa-

ration presented 10-fold more of these groups to the A $\beta$  peptides in each such experiment than did the monomer fraction. Thus, it is not surprising that oligomers were the most potent inhibitors. Conversely, if the number of phenolic hydroxyl groups in each inhibitor preparation were equal, then the results therefrom cannot depend on absolute number of phenolic hydroxyl groups *per se*. Instead, the results should depend on the structure of the inhibitor examined.

Eisenberg and coworkers have sought an answer to the question of how assembly inhibitors bind to A $\beta$ . To do so, they determined the X-ray crystallographic structures of amyloid forming segments of A $\beta$  and Tau in complex with small molecules. They proposed a model of interaction wherein various aromatic compounds, such as polyphenols, would bind to a variety of amyloid-forming sequences within a cylindrical, partially apolar cavity between the pairs of  $\beta$ -sheets forming the fibers, which can also be present in oligomeric structures of A $\beta$  (Landau *et al.* 2011). If we consider this model with respect to our finding that GSPE monomer is the most potent inhibitor of A $\beta$  assembly (when equal weights of GSPE are compared), then the low inhibitory activity of GSPE oligomers could be due to their size, which precludes their accessing these cavities between  $\beta$ -sheets.

To visualize potential-binding modes of GSPE and A $\beta$ 40, we created models of complexes formed between A $\beta$ 40

**Fig. 7** Grape seed polyphenolic extract (GSPE):A $\beta$  interactions. A model of GSPE:A $\beta$  interactions was created to illustrate the potential differences between systems in which GSPE fractions were studied at *equimolar* concentrations or at *equal weight* concentrations. A partially folded A $\beta$ 40 structure, derived using solution-state NMR (PDB: 2LFM), is shown as a semi-transparent surface where red represents negative charges near the surface and blue represents positively charged regions. The white regions correspond to essentially neutral potentials. The protein backbone is displayed using a ribbon representation. GSPE monomer (green) or oligomer (blue) are shown as stick structures, in which red represents oxygen and white represents hydrogen. Panels are: (a) A single monomer docked to A $\beta$ 40; (b) four monomers docked to A $\beta$ 40; and (c) a single oligomer docked to A $\beta$ 40. Comparison between (a) and (c) illustrates equal molarity of GSPE's whereas comparison between (b) and (c) illustrates equal masses of GSPEs.



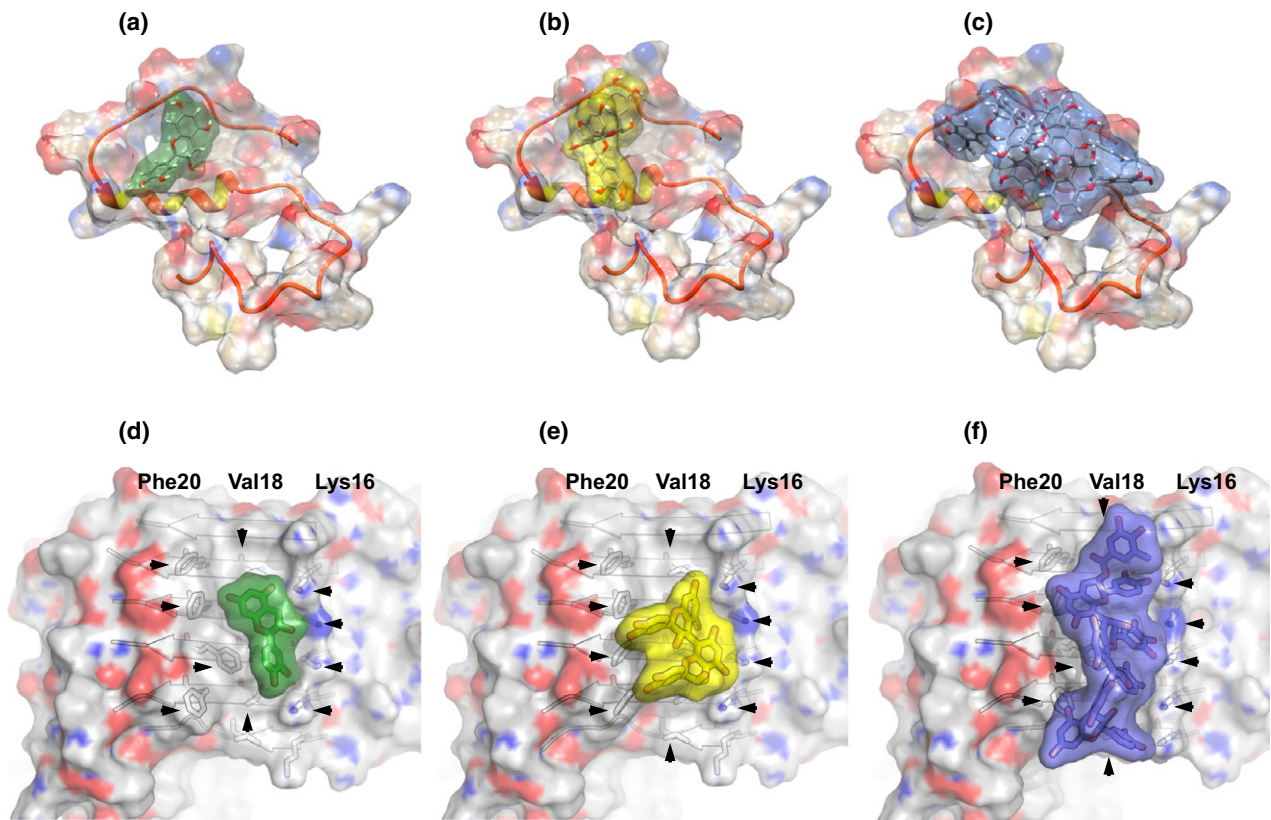


**Fig. 8** Models of complexes between Aβ40 and grape seed polyphenolic extract (GSPE) monomers, dimers or oligomers. Panels are: (a) docked monomer, (b) docked dimer, and (c) docked oligomer. The peptide backbone is illustrated in orange and red. Panels d–f show the monomer (d), dimer (e), and oligomer (f) interacting with backbone

atoms of an Aβ fibril. Fibril side-chains are shown in gray and extend from β-strands oriented equatorially relative to the fibril axis. Hydroxyl groups form hydrogen bonds to Lys16 of Aβ. Apolar interactions may occur among the aromatic rings of GSPE and the hydrophobic patches formed by Val18 and Phe20 of Aβ.

(Vivekanandan *et al.* 2011) and GSPE monomer, dimer, or oligomer (Figs 7 and 8). GSPE monomer and dimer were docked to a partially structured Aβ40 (Protein Data Bank (PDB) entry: 2LFM) (Vivekanandan *et al.* 2011) using SwissDock. GSPE oligomer has been placed in one possible binding location for comparison. Figure 7a and c allow comparison of binding modes for equal *moles* of monomer and oligomer. Figure 7b and c allow comparison of binding modes for equal *weights* of monomer and oligomer. Four monomers can explore a larger percentage of the Aβ surface than can the single oligomer because of the lack of conformational freedom imposed on the latter structure by its rigidity. A useful metaphor for this idea is the relative numbers of intermolecular contacts possible between a sphere exploring the uneven Aβ surface versus a plane exploring the surface. The sphere can make many more contacts than can the plane because it can contact surfaces within relatively small depressions that the plane is precluded from accessing because of its planar geometry.

We also explored the ability of GSPE monomer, dimer, and oligomer to interact with a fibril model (PDB entry:

2LMO) (Petkova *et al.* 2006) of Aβ, using Rosetta docking simulations, as described previously (Jiang *et al.* 2013). These interactions are shown in Fig. 8d–f, along with the surface-binding modes shown in Fig. 7a for comparison (Fig. 8a–c). Interatomic interactions on the face of a fibril model are shown in Figure S2. Here, interactions are observed between the GSPE molecules and the side chains of Phe20, Val18, and Lys16 on Aβ. GSPE hydroxyl groups form hydrogen bonds to Lys16. The surface representation highlights complementary apolar interactions between the aromatic rings of GSPE and the hydrophobic patches formed by Val18 and Phe20 of Aβ.

The interaction of the GSPE monomer with Lys16, Val18, and Phe20 is similar to that observed in co-crystals of Orange G bound to the KLVFFA fibril-forming segment of Aβ (Landau *et al.* 2011). Here, Orange G is bound internally to the steric zipper, corresponding to residues 16–21 of Aβ, and displays polar interactions with Lys16 and hydrophobic interactions with Leu17, Val18, Phe19, and Phe20. In the case of the GSPE dimer, binding interactions are also similar to those of Landau *et al.* (Landau *et al.* 2011) but the relative

energy contributions of polar and hydrophobic interactions differ. The fibril binding of GSPE dimer is stabilized mainly through hydrophobic interactions with Val 18 and 20, while polar hydrogen bonding to Lys 16 is poor because its hydrogen bond geometry is not ideal.

Our studies emphasize the importance of considering how the molecular weight of each GSPE fraction might affect its potential therapeutic utility *in vivo*, where the blood-brain barrier is involved in controlling the permeability of molecules into the brain (Wang *et al.* 2012). The monomer fraction is able to cross the blood brain barrier (Wang *et al.* 2012) and a metabolite of the GSPE monomer promoted basal synaptic transmission and long-term potentiation at physiologic concentrations in hippocampal slices (Wang *et al.* 2012). Indeed, GSPE proanthocyanidins are absorbed in the gastrointestinal tract and display no toxicity in rats at a 2.5% (w/w) concentration. GSPE monomer does appear to have greater bioavailability relative to larger GSPE components (Bentivegna and Whitney 2002; Ferruzzi *et al.* 2009; Wang *et al.* 2012). Taken together with the fact that monomers appear to be the most effective A $\beta$  assembly inhibitors, as shown in the studies presented in this manuscript, monomers appear to be the most promising form of GSPE for clinical study.

### Acknowledgments and conflict of interest disclosure

We thank Dr. Zhefeng Gou for helpful discussions. This work was supported by grants from the UCLA Chemistry–Biology Interface (CBI) Training Program, UCLA Training Program in Neural Repair, Jim Easton Consortium for Alzheimer’s Drug Discovery, and Biomarkers at UCLA, and NIH grants AG027818, NS038328, and AG041295. This study was supported in part through support from the NCCIH Center Grant 1PO1AT004511-031 to GMP. Dr. Pasinetti holds a Career Scientist Award in the Research and Development unit and is the Director of the Basic and Biomedical Research and Training Program, GRECC, James J. Peters Veterans Affairs Medical Center. We acknowledge that the contents of this article do not represent the views of the U.S. Department of Veterans Affairs or the United States Government. Drs. Pasinetti, Wang, and Ho are named inventors on a patent filed through the Icahn School of Medicine at Mount Sinai for the use of grape seed extract for the treatment of Alzheimer’s disease and other neurodegenerative disorders. Drs Pasinetti, Wang, and Ho are entitled to receive royalties from this invention.

### Author contributions

EYH, GY, SB, and BC carried out the experiments. EYH, GY, SB, and DBT wrote the manuscript. MK and LJ carried out the docking and model building. LH, JW, and GMP provided the fractionated GSPE. EYH, GY, GMP, and DBT designed the studies. All authors have given approval of the final version of the manuscript.

### Supporting information

Additional supporting information may be found in the online version of this article at the publisher’s web-site:

**Figure S1.** Three-dimensional structures of the GSPE monomer, dimer, and oligomer, shown in Fig. 1.

**Figure S2.** Structural models of GSPE:fibril interactions.

**Table S1.** Energetics of GSPE:A $\beta$  complexation.

### References

- Ferri C. P., Sousa R., Albanese E., Ribeiro W. S., & Honyashiki M. (2009) World Alzheimer Report 2009–Executive Summary. Edited by: Prince M, Jackson J. London: Alzheimer’s Disease International, 1–22.
- Bentivegna S. S. and Whitney K. M. (2002) Subchronic 3-month oral toxicity study of grape seed and grape skin extracts. *Food Chem. Toxicol.* **40**, 1731–1743.
- Bitan G., Lomakin A. and Teplow D. B. (2001) Amyloid  $\beta$ -protein oligomerization: prenucleation interactions revealed by photo-induced cross-linking of unmodified proteins. *J. Biol. Chem.* **276**, 35176–35184.
- Bitan G., Kirkitadze M. D., Lomakin A., Vollers S. S., Benedek G. B. and Teplow D. B. (2003) Amyloid  $\beta$ -protein (A $\beta$ ) assembly: A $\beta$ 40 and A $\beta$ 42 oligomerize through distinct pathways. *Proc. Natl Acad. Sci. USA* **100**, 330–335.
- Brookmeyer R., Johnson E., Ziegler-Graham K. and Arrighi H. M. (2007) Forecasting the global burden of Alzheimer’s disease. *Alzheimers Dement.* **3**, 186–191.
- Cummings J. L. (2004) Alzheimer’s disease. *N. Engl. J. Med.* **351**, 56–67.
- Davis I. W. and Baker D. (2009) RosettaLigand docking with full ligand and receptor flexibility. *J. Mol. Biol.* **385**, 381–392.
- Dorozynski A. (1997) Wine may prevent dementia. *Br. Med. J.* **314**, 997.
- Fancy D. A. and Kodadek T. (1999) Chemistry for the analysis of protein–protein interactions: rapid and efficient cross-linking triggered by long wavelength light. *Proc. Natl Acad. Sci. USA* **96**, 6020–6024.
- Ferruzzi M. G., Lobo J. K., Janle E. M. *et al.* (2009) Bioavailability of gallic acid and catechins from grape seed polyphenol extract is improved by repeated dosing in rats: implications for treatment in Alzheimer’s disease. *J. Alzheimers Dis.* **18**, 113–124.
- Flamini R. (2003) Mass spectrometry in grape and wine chemistry. *Mass Spectrom. Rev.* **22**, 218–250.
- Fletcher D. A., McMeeking R. F. and Parkin D. (1996) The United Kingdom chemical database service. *J. Chem. Inf. Comp. Sci.* **36**, 746–749.
- Gazova Z., Siposova K., Kurin E., Mucaji P. and Nagy M. (2013) Amyloid aggregation of lysozyme: the synergy study of red wine polyphenols. *Proteins* **81**, 994–1004.
- Groenning M. (2010) Binding mode of Thioflavin T and other molecular probes in the context of amyloid fibrils-current status. *J. Chem. Biol.* **3**, 1–18.
- Grosdidier A., Zoete V. and Michielin O. (2011a) Fast docking using the CHARMM force field with EADock DSS. *J. Comput. Chem.* **32**, 2149–2159.
- Grosdidier A., Zoete V. and Michielin O. (2011b) SwissDock, a protein-small molecule docking web service based on EADock DSS. *Nucleic Acids Res.* **39**, W270–W277.
- Hardy J. A. and Higgins G. A. (1992) Alzheimer’s disease: the amyloid cascade hypothesis. *Science* **256**, 184–185.

- Ho L., Yemul S., Wang J. and Pasinetti G. (2009) Grape seed polyphenolic extract as a potential novel therapeutic agent in tauopathies. *J. Alzheimers Dis.* **16**, 433–439.
- Jiang L., Liu C., Leibly D., Landau M., Zhao M., Hughes M. P. and Eisenberg D. S. (2013) Structure-based discovery of fiber-binding compounds that reduce the cytotoxicity of amyloid beta. *eLife*, **2**, e00857.
- Kirkitaдзе M. D., Condrón M. M. and Teplow D. B. (2001) Identification and characterization of key kinetic intermediates in amyloid  $\beta$ -protein fibrillogenesis. *J. Mol. Biol.* **312**, 1103–1119.
- Klein W. E. (2006) Cytotoxic intermediates in the fibrillation pathway: A $\beta$  oligomers in Alzheimer's disease as a case study, in *Part A: Protein Misfolding, Aggregation, and Conformational Diseases*, Vol. 4, (Uversky V. N. and Fink A. L., eds), pp. 61–75. Springer, New York.
- Kumar V., Kumar C. S., Hari G., Venugopal N. K., Vijendra P. D. and B G. B. (2013) Homology modeling and docking studies on oxidosqualene cyclases associated with primary and secondary metabolism of *Centella asiatica*. *SpringerPlus*, **2**, 189.
- Landau M., Sawaya M. R., Faull K. F., Laganowsky A., Jiang L., Sievers S. A., Liu J., Barrio J. R. and Eisenberg D. (2011) Towards a pharmacophore for amyloid. *PLoS Biol.* **9**, e1001080.
- Lawrence M. C. and Colman P. M. (1993) Shape complementarity at protein/protein interfaces. *J. Mol. Biol.* **234**, 946–950.
- Letenneur L., Dartigues J. F. and Orgogozo J. M. (1993) Wine consumption in the elderly. *Ann. Intern. Med.* **118**, 317–318.
- Meiler J. and Baker D. (2006) ROSETTALIGAND: protein-small molecule docking with full side-chain flexibility. *Proteins* **65**, 538–548.
- Ochs D. (1983) Protein contaminants of sodium dodecyl sulfate-polyacrylamide gels. *Anal. Biochem.* **135**, 470–474.
- Ono K., Condrón M. M., Ho L., Wang J., Zhao W., Pasinetti G. M. and Teplow D. B. (2008) Effects of grape seed-derived polyphenols on amyloid  $\beta$ -protein self-assembly and cytotoxicity. *J. Biol. Chem.* **283**, 32176–32187.
- Orgogozo J. M., Dartigues J. F., Lafont S., Letenneur L., Commenges D., Salamon R., Renaud S. and Breteler M. B. (1997) Wine consumption and dementia in the elderly: a prospective community study in the Bordeaux area. *Rev. Neurol. (Paris)* **153**, 185–192.
- Orlando R. A., Gonzales A. M., Royer R. E., Deck L. M. and Vander Jagt D. L. (2012) A chemical analog of curcumin as an improved inhibitor of amyloid A $\beta$  oligomerization. *PLoS ONE* **7**, e31869.
- Pasinetti G. M., Ksiezak-Reding H., Santa-Maria I., Wang J. and Ho L. (2010) Development of a grape seed polyphenolic extract with anti-oligomeric activity as a novel treatment in progressive supranuclear palsy and other tauopathies. *J. Neurochem.* **114**, 1557–1568.
- Petkova A. T., Yau W. M. and Tycko R. (2006) Experimental constraints on quaternary structure in Alzheimer's  $\beta$ -amyloid fibrils. *Biochemistry* **45**, 498–512.
- Roychaudhuri R., Yang M., Hoshi M. M. and Teplow D. B. (2009) Amyloid  $\beta$ -protein assembly and Alzheimer disease. *J. Biol. Chem.* **284**, 4749–4753.
- Sharma V., Zhang C. F., Pasinetti G. M. and Dixon R. A. (2011) Fractionation of grape seed proanthocyanidins for bioactivity assessment in D.R. Gang (ed.), *The Biological Activity of Phytochemicals, Recent Advances in Phytochemistry* **41**, DOI 10.1007/978-1-4419-7299-6\_3, Springer Science+Business Media, LLC 2011.
- Sinha S., Lopes D. H., Du Z. *et al.* (2011) Lysine-specific molecular tweezers are broad-spectrum inhibitors of assembly and toxicity of amyloid proteins. *J. Am. Chem. Soc.* **133**, 16958–16969.
- Teplow D. B. (2006) Preparation of amyloid  $\beta$ -protein for structural and functional studies. *Meth Enzymol* **413**, 20–33.
- Teplow D. B., Lazo N. D., Bitan G. *et al.* (2006) Elucidating amyloid  $\beta$ -protein folding and assembly: a multidisciplinary approach. *Acc. Chem. Res.* **39**, 635–645.
- Truelsen T., Thudium D. and Gronbaek M. (2002) Amount and type of alcohol and risk of dementia: the Copenhagen City Heart Study. *Neurology* **59**, 1313–1319.
- Turner R. J. and Charlton S. J. (2005) Assessing the minimum number of data points required for accurate IC<sub>50</sub> determination. *Assay Drug Dev. Technol.* **3**, 525–531.
- Virgili M. and Contestabile A. (2000) Partial neuroprotection of *in vivo* excitotoxic brain damage by chronic administration of the red wine antioxidant agent, trans-resveratrol in rats. *Neurosci. Lett.* **281**, 123–126.
- Vivekanandan S., Brender J. R., Lee S. Y. and Ramamoorthy A. (2011) A partially folded structure of amyloid-beta(1-40) in an aqueous environment. *Biochem. Biophys. Res. Commun.* **411**, 312–316.
- Walsh D. M., Lomakin A., Benedek G. B., Condrón M. M. and Teplow D. B. (1997) Amyloid  $\beta$ -protein fibrillogenesis. Detection of a protofibrillar intermediate. *J. Biol. Chem.* **272**, 22364–22372.
- Wang J., Ho L., Zhao W., Ono K., Rosensweig C., Chen L., Humala N., Teplow D. B. and Pasinetti G. M. (2008) Grape-derived polyphenolics prevent A $\beta$  oligomerization and attenuate cognitive deterioration in a mouse model of Alzheimer's disease. *J. Neurosci.* **28**, 6388–6392.
- Wang J., Ferruzzi M. G., Ho L. *et al.* (2012) Brain-targeted proanthocyanidin metabolites for Alzheimer's disease treatment. *J. Neurosci.* **32**, 5144–5150.



## **Inhibiting amyloid $\beta$ -protein assembly: Size-activity relationships among grape seed-derived polyphenols**

***Eric Y. Hayden<sup>#, 1</sup>, Ghiam Yamin<sup>#, 1, 2, 3</sup>, Shiela Beroukhim<sup>1</sup>, Benson Chen<sup>1</sup>, Mikhail Kibalchenko<sup>1</sup>, Lin Jiang<sup>1</sup>, Lap Ho<sup>4</sup>, Jun Wang<sup>4,5</sup>, Giulio M. Pasinetti<sup>4,5</sup> and David B. Teplow<sup>\*, 1, 6</sup>***

<sup>1</sup>Department of Neurology, David Geffen School of Medicine, University of California, Los Angeles, CA

<sup>2</sup>Medical Scientist Training Program, Neuroscience Interdepartmental Ph.D. Program, University of California, Los Angeles, CA 90095

<sup>4</sup>Departments of Psychiatry and Neuroscience, Icahn School of Medicine at Mount Sinai, NY, NY 10029

<sup>5</sup>Department of Neurology, Icahn School of Medicine at Mount Sinai, One Gustave L. Levy Place, New York, NY, Geriatric Research, Education and Clinical Center (GRECC), James J. Peters Veterans Affairs Medical Center, 130 West Kingsbridge Road, Bronx, NY

<sup>6</sup>Molecular Biology Institute (MBI), and Brain Research Institute (BRI), David Geffen School of Medicine, University of California, Los Angeles, CA 90095

<sup>#</sup>These authors contributed equally to this work.

<sup>3</sup>Present address: Department of Radiology, University of California, San Diego

\*Correspondence should be addressed to: David B. Teplow, Tel.: 310-206-2030, Fax: 310-206-1700, E-mail: [dteplow@mednet.ucla.edu](mailto:dteplow@mednet.ucla.edu)

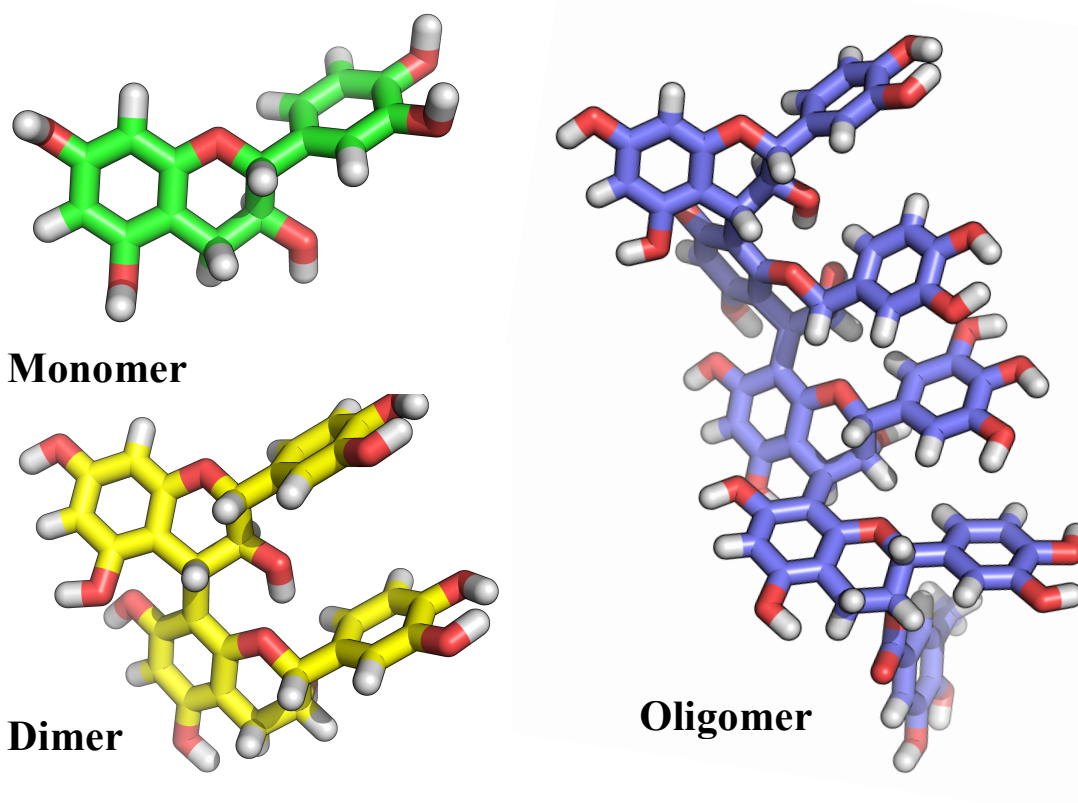


**Fig. S1. Three-dimensional structures of the GSPE monomer, dimer, and oligomer, shown in Fig. 1. Monomer (green), dimer (yellow), and oligomer (purple) are shown as stick models with oxygen atoms shown in red and hydrogen atoms shown in white.**

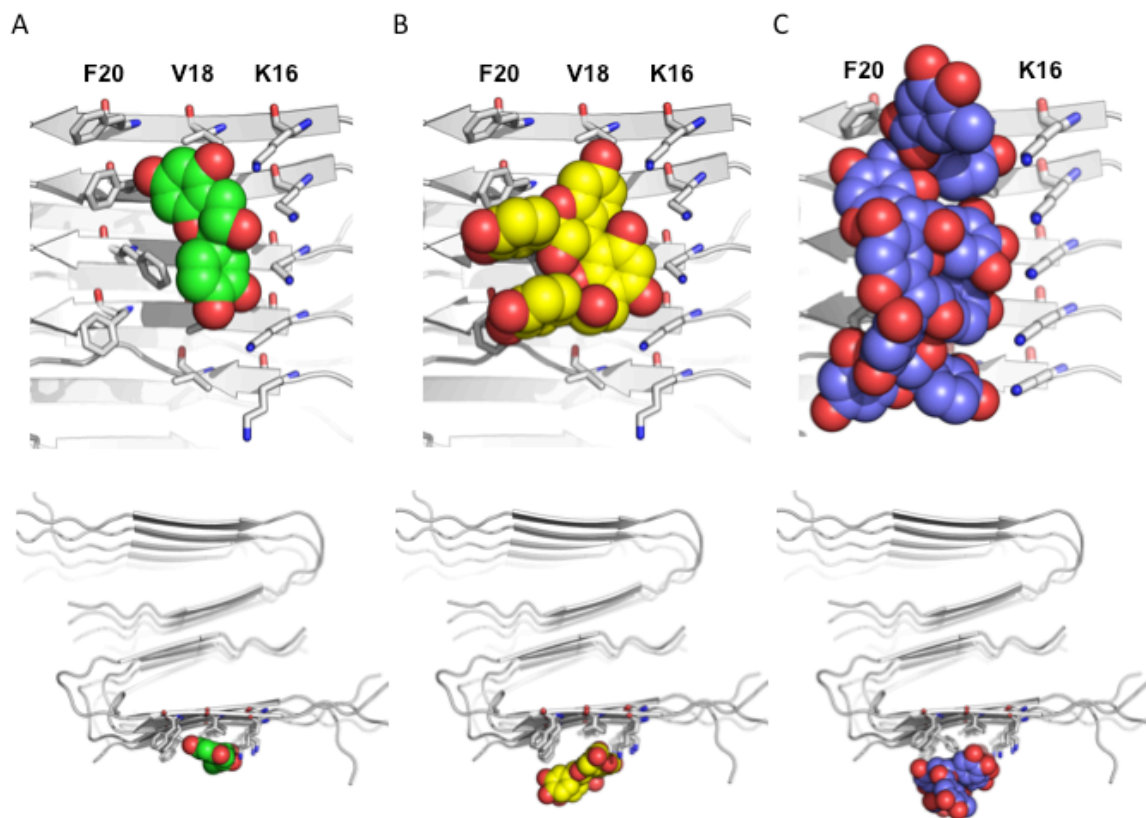


**Fig. S2. Structural models of GSPE:fibril interactions.** Monomer (A), dimer (B), and oligomer (C) are docked on an A $\beta$  fibril (grey) whose fibril axis extends from the bottom to the top of the figure (top row of figures). These same interactions are viewed looking down the fibril axis in the bottom row of figures. A $\beta$  fibril side-chains are shown in stick representation.

**Table S1. Energetics of GSPE:A $\beta$  complexation<sup>a</sup>**

<b>GSPE</b>	<b>Binding Energy</b>	<b>Non-bond Potential<sup>b</sup></b>	<b>Solvation Energy<sup>c</sup></b>	<b>Electrostatic Potential<sup>d</sup></b>	<b>H-bond Energy<sup>e</sup></b>
<b>Monomer</b>	-9	-9	3	-1	-2
<b>Dimer</b>	-10	-13	5	0	-1
<b>Oligomer</b>	-18	-23	10	-1	-4

**Table S1.** Energetics of GSPE:A $\beta$  complexation. A comparison of the predicted binding energy and physically meaningful energy terms of each model.

<sup>a</sup>- Energies are listed as kcal/mol.

<sup>b</sup>- The attractive portion of the non-bonded Lennard-Jones potential (1).

<sup>c</sup>- LK implicit solvation energy (2).

<sup>d</sup>- Simple Coulombic electrostatics (1).

<sup>e</sup>- Interfacial hydrogen binding energy (3).

1. Brooks B.R., Bruccoleri R.E., Olafson B.D., States D.J., Swaminathan S. (1983) CHARMM: a program for macromolecular energy, minimization, and dynamics calculations. *J Comp Chem*, **4**, 187-217.

2. Lazaridis T, Karplus M. (1999) Effective energy function for proteins in solution. *Proteins*, **35**, 133-152.

3. Kortemme T, Morozov AV, Baker D. (2003) An orientation-dependent hydrogen bonding potential improves prediction of specificity and structure for proteins and protein–protein complexes. *J Mol Biol* **326**, 1239-1259.